Remote Sensing of Forest Biomass Using GNSS Reflectometry

Emanuele Santi ⓘ, *Member, IEEE*, Simonetta Paloscia ⓘ, *Fellow, IEEE*, Simone Pettinato, *Member, IEEE*, Giacomo Fontanelli, Maria Paola Clarizia, *Senior Member, IEEE*, Davide Comite ⓘ, *Member, IEEE*, Laura Dente ⓘ, Leila Guerriero ⓘ, *Member, IEEE*, Nazzareno Pierdicca ⓘ, *Senior Member, IEEE*, and Nicolas Floury ⓘ

Abstract—In this study, the capability of Global Navigation Satellite System Reflectometry in evaluating forest biomass from space has been investigated by using data coming from the TechDemoSat-1 (TDS-1) mission of Surrey Satellite Technology Ltd. and from the Cyclone Satellite System (CyGNSS) mission of NASA. The analysis has been first conducted using TDS-1 data on a local scale, by selecting five test areas located in different parts of the Earth's surface. The areas were chosen as examples of various forest coverages, including equatorial and boreal forests. Then, the analysis has been extended by using CyGNSS to a global scale, including any type of forest coverage. The peak of the Delay Doppler Map calibrated to retrieve an "equivalent" reflectivity has been exploited for this investigation and its sensitivity to forest parameters has been evaluated by a direct comparison with vegetation optical depth (VOD) derived from the Soil Moisture Active Passive L-band radiometer, with a pantropical aboveground biomass (AGB) map and then with a tree height (H) global map derived from the Geoscience Laser Altimeter System installed on-board the ICEsat satellite. The sensitivity analysis confirmed the decreasing trend of the observed equivalent reflectivity for increasing biomass, with correlation coefficients $0.31 \leq R \leq 0.54$ depending on the target parameter (VOD, AGB, or H) and on the considered dataset (local or global). These correlations were not sufficient to retrieve the target parameters by simple inversion of the direct relationships. The retrieval has been therefore based on Artificial Neural Networks making it possible to add other inputs (e.g., the incidence angle, the signal to noise ratio, and the lat/lon information in case of global maps) to the algorithm. Although not directly correlated to the biomass, these inputs helped in improving the retrieval accuracy. The algorithm was tested on both the selected areas and globally, showing a promising ability to retrieve the target parameter, either AGB or H, with correlation coefficients $R \simeq 0.8$.

Index Terms—Artificial neural networks (ANNs), Cyclone Satellite System (CyGNSS), forest biomass, Global Navigation Satellite System (GNSS) Reflectometry, Soil Moisture Active Passive (SMAP), TechDemoSat-1 (TDS-1).

I. INTRODUCTION

GLOBAL Navigation Satellite System (GNSS) Reflectometry (GNSS-R) represents a valuable tool for remote sensing key bio-geophysical parameters [1], [2]. Besides ocean surface applications (wind and wave, sea surface height), e.g., [3], land applications based on GNSS-R are also emerging, including the retrieval of soil moisture and forest aboveground biomass (AGB), which are essential variables for the understanding of the hydrological and carbon cycles [4]–[7]. GNSS-R has in fact some advantages with respect to other currently used methods to estimate soil moisture and vegetation biomass. First, GNSS signals are transmitted at L-band, which is a spectral region highly sensitive to the water content of the observed target, with a considerable penetration and therefore capable to sense, e.g., the soil under vegetation [8]. Second, unlike microwave radiometry, thermal background variations do not dramatically contaminate the GNSS-reflected signals. Third, GNSS-R has potentially higher spatial resolution than microwave radiometry, due to the highly stable modulation of the navigation signals, which enable the implementation of delay Doppler discrimination [9], [10].

This study includes data acquired by the TechDemoSat-1 (TDS-1) mission of Surrey Satellite Technology Ltd. (SSTL), launched in 2014 [11], and by the NASA's Cyclone GNSS (CyGNSS), launched in 2017 [12]. Among the other mission studies, we can cite the ESA's GNSS-R Radio Occultation and Scatterometry Experiment Onboard the International Space Station [13], and the ESA's Passive Reflectometry and Interferometry System In-Orbit Demonstrator [14], but other initiatives are being carried out.

The GNSS-R signal from land is constituted by both nearly specular reflection from the soil surface and diffuse scattering from surface roughness and vegetation. The sensitivity of specularly reflected signals to AGB was predicted by electromagnetic models, as the specular reflection from the soil of the impinging L-band signal is expected to be attenuated by the vegetation because of its optical depth [15]. The Bi-MIMICS simulator also suggested a better sensitivity of bistatic than monostatic

Emanuele Santi, Simonetta Paloscia, Simone Pettinato, and Giacomo Fontanelli are with the Institute of Applied Physics, National Research Council, Florence 50019, Italy (e-mail: e.santi@ifac.cnr.it; s.paloscia@ifac.cnr.it; simone.pettinato@ifac.cnr.it; g.fontanelli@ifac.cnr.it).

Maria Paola Clarizia is with the Deimos Space UK, Didcot OX11 0QR, U.K. (e-mail: mariapaola.clarizia@deimos-space.com).

Davide Comite and Nazzareno Pierdicca are with the Department of Information Engineering, Electronics and Telecommunications, La Sapienza University of Rome, Rome 00184, Italy (e-mail: davide.comite@uniroma1.it; nazzareno.pierdicca@uniroma1.it).

Laura Dente and Leila Guerriero are with the Dipartimento di Ingegneria Civile e Ingegneria Informatica, University of Rome Tor Vergata, Rome 00133, Italy (e-mail: laura.dente@uniroma2.it; leila.guerriero@uniroma2.it).

Nicolas Floury is with the European Space Agency–European Space Research and Technology Center, Noordwijk 2201 AZ, the Netherlands (e-mail: nicolas.floury@esa.int).

Digital Object Identifier 10.1109/JSTARS.2020.2982993

configurations [16]. The experiments conducted from 2008 to 2012 during the ESA projects GRASS and Leimon demonstrated that cross polarized reflectivity Γ_{RL}, defined as the ratio between reflected and direct power, measured from ground and airborne platforms was sensitive to vegetation biomass, exhibiting a monotonic decrease [17], [18].

The sensitivity to woody biomass of poplar plots observed during the GRASS experiment was around $1.5\ 10^{-2}$ dB(t/ha)$^{-1}$, with a correlation coefficient $R = 0.91$. These findings were confirmed by an airborne experimental campaign conducted over Les Landes forest [19]. In that case, it was observed an even larger sensitivity of about $5\ 10^{-2}$ dB(t/ha)$^{-1}$, which however was limited to very high elevation angles, in the range 70°–90°. It is interesting to note that a saturation effect was not observed within the AGB values considered in the analysis. This could represent a major improvement with respect to conventional monostatic radars, since the backscattering coefficient at L-band is reported to saturate for biomass higher than 100–150 t/ha, depending on the type of forest [20].

Forest observations were carried out from a stratospheric balloon at about 25-km height, as reported in [21]. The experiment evidenced a strong coherent component, singled out by a long coherent integration time (20 ms), which was associated mainly to soil reflection, but also to vegetation and soil–vegetation interaction.

As for satellite data, extensive analyses of TDS-1 and CyGNSS data were carried out in [22]–[24], comparing the GNSS-R observables with vegetation-related parameters. A negative correlation of TDS-1 SNR with the Normalized Differential Vegetation Index was observed in [22] (Fig. 16). The comparison of CyGNSS reflectivity with the Soil Moisture Active and Passive (SMAP) vegetation opacity product also showed a correlation predominantly negative [Fig. 8(b) in [23]]. Finally, in [24], the authors analyzed the relationship between biomass and tree height by computing the zero Doppler waveform trailing edge (TE) from CyGNSS data.

Based on these results, this study aims at further investigating the sensitivity of the GNSS-R signal collected from space to vegetation biomass, and especially at assessing the possibility of estimating this parameter using data from satellite, namely those delivered by TDS-1 and CyGNSS.

In this study, the sensitivity of GNSS-R observables to different forest parameters was first assessed at a local scale by using TDS-1 data, and then extended to a global scale, by using CyGNSS data. In particular, as for the local analysis, five test areas located in different parts of the Earth's surface were identified, as examples of the most important forest types, from boreal to equatorial forests. The local analysis considered the peak of the Delay Doppler Map (DDM) from which two observables were derived, i.e., an equivalent reflectivity (Γ) and the signal to noise ratio (SNR), confirming that Γ is the parameter more correlated to the vegetation biomass, as previously demonstrated for soil moisture (e.g., [25]). Note that the peak of the DDM exploited in this article is affected by both the specularly reflected component and the scattered diffuse component, whereas other observables, such as the TE, are uniquely affected by the diffuse term [24].

The comparison also included data acquired by the second generation of Phased Array type L-band Synthetic Aperture Radar (PALSAR-2), on board of the Advanced Land Observing Satellite (ALOS), collected on the same areas and in the same period of GNSS-R data, to provide a reference and to compare the performances of monostatic radar versus GNSS-R. As reference information for evaluating the sensitivity of GNSS-R observables to forest on a global scale, three datasets were selected: the SMAP Vegetation Optical Depth (VOD) [26], the improved pantropical biomass map (Dry Biomass in t/ha) [27] and the global map of tree height derived from the Geoscience Laser Altimeter System installed on-board the ICEsat satellite (ICE-GLAS) satellite LiDAR [28].

Although VOD is an electromagnetic parameter rather than a biophysical one, and height is not strictly providing the biomass, their easy availability on a global scale makes those parameters worth being considered as proxy to biomass for sensitivity assessment.

The study was carried out on the five test areas by using TDS-1 and then extended to the global scale by using CyGNSS. This strategy was selected due to the poor TDS-1 coverage at global scale (TDS-1 is a technology demonstrator, which did not operate continuously) and on the CyGNSS constellation acquisitions limited to the ±38° latitude range. An intercomparison of the two sensors on a set of common data was also carried out to point out different behaviors and sensitivities.

Based on the encouraging results of the sensitivity analysis, the GNSS-R capability of estimating the forest biomass was exploited by implementing and testing retrieval algorithms based on Artificial Neural Networks (ANN).

This study confirmed the fairly good sensitivity of GNSS-R data to the target forest parameter, namely AGB, tree height, and VOD, and demonstrated the potential of GNSS-R for the forest biomass monitoring.

The article is structured as follows: the test areas, the satellite, and the reference datasets considered in this study are described in Section II. The sensitivity of GNSS-R observables to the forest biomass, conducted at local and global scales, is described and discussed in Section III. The biomass retrieval is attempted in Section IV: this section describes the implementation of the retrieval algorithms and the results obtained at local scale using TDS-1 data and at global scale using CyGNSS. Conclusions are drawn in Section V.

II. TEST AREAS AND DATASETS

The main characteristics of the five test areas, the datasets investigated in this study, as well the relevant preprocessing tasks are described in this section.

A. GNSS-R Data Preprocessing

The GNSS-R received power is made up of a near specular reflection from the mean soil surface and a diffuse scattering from soil roughness and vegetations [29], [30]. The specular reflection, attenuated by the vegetation, is generally associated to the coherent term and the diffuse component to the incoherent

one, although the actual degree of coherence of those components is subject of recent investigations [10]. Being interested in the attenuation of the specular reflection from the soil and following the prevailing approach when dealing with GNSS-R data acquired over land, in this study, we have considered as observable the peak of the DDM, which has been calibrated by computing an equivalent reflectivity of the Earth's surface Γ. It assumes the received power is expressed by the radar equation for an equivalent plane surface producing the same power actually originated by specular and diffuse contributions from soil and vegetation [31]–[34]. The incoherent contribution to the measured signal (e.g., from soil and vegetation volume scattering) acts as a nuisance terms with respect to this assumption.

On this basis, the power received by the down-looking antenna can be written as

$$P_r^S = \Gamma(\theta) \frac{\lambda^2 G^t G^r P_t}{(4\pi)^2 (R_r + R_t)^2} \qquad (1)$$

where R_r is the distance from receiver to the specular point (SP), R_t from transmitter to SP, λ is the wavelength, G^t and G^r are the gain of transmitting and receiving (i.e., down-looking) antennas, and P_t is the transmitted power. Γ is the Earth's surface equivalent reflectivity, which is a function of the incidence angle θ at the SP. The equivalent reflectivity embeds the effects of soil moisture content, small-scale roughness, and eventual attenuation introduced by the vegetation cover, as well as any contribution of the incoherent scattering. To retrieve the unknown transmitter Equivalent Isotropic Radiate Power $EIRP = G^t P_t$, we followed different approaches, according to the data available in the TDS-1 and CyGNSS products.

In case of TDS-1, the EIRP is not provided, so we exploited the amplitude of the direct signal collected by the up-looking antenna as described in [35]. The Γ parameter is retrieved from the peak power P_r^* of the DDM, the DDM noise N^* estimated from the first delay lines preceding the peak, the direct power P_d^*, and the related noise N_d^* through the following formula:

$$\Gamma(\theta) = \frac{(R_r + R_t)^2}{R_{rt}^2} \frac{(P_r^* - N^*)}{(P_d^* - N_d^*)} \frac{G_{UP}^r}{G^r}. \qquad (2)$$

R_{rt}^2 is the distance from transmitter to receiver, the gain G^r toward the SP is extracted from the L1b product, whereas as for the upward antenna gain G_{UP}^r, we considered a constant nominal value of 4 dB, assuming a very wide pattern, according to the Measurement of Earth Reflected Radio-navigation signals By Satellite (Merrbys) documentation (http://merrbys.co.uk/).

The approach may have drawbacks since it would require a good knowledge of the up-looking antenna pattern, as well as of the relative gain of the receiving chains collecting the reflected and direct signals [35]. A wrong characterization of the angular dependence of Γ could be introduced by errors in the down-looking antenna pattern due to attitude uncertainty, as well as the lack of information on the pattern of the up-looking antenna.

In case of CyGNSS, only the SNR is given for the direct signal in the L1b products. If it was used to normalize the reflected

TABLE I
LIST OF THE TEST AREAS CONSIDERED FOR THIS STUDY

TEST AREA	LAT (deg)	LON (deg)	Forest Type
Brazil (Manaus)	-6/-2	-61.5/-58	flooded equatorial
Uruguay (Algorta)	-33/-32	-57.8/-57	dense coniferous
Alaska (Fairbanks)	63/67.5	-152/-143	boreal open
Finland	65.5/69.5	20/30	boreal open
Argentina (Asuncion)	-26/-22	-63/-59	mixed

signal power in the computation of Γ, the zenith noise will remain unknown in the calibration formula (1). Moreover, the automatic gain control in the direct signal receiver, operating till Summer 2018 is another reason hampering the use of the direct signal in CyGNSS. Then, we used the EIRP value that is provided in the products, as done e.g., in [7].

The quality of absolute calibration is a well-known issue in spaceborne GNSS-R. For this reason, we also included the $SNR = (P_r^*/N^* - 1)$ in the analysis and compared the sensitivity of both observables, i.e., Γ and SNR. It was found that Γ is more correlated to the target vegetation parameters than SNR, so we will consider Γ as the main observable in the following sensitivity analysis.

Considering the uncertainty in the satellite attitude and antenna patterns required in (1), data collected at incidence angles higher than 45° were discarded: this threshold has been set as a compromise between the need of limiting measurements at the edge or outside the antenna main beam and, again, the need of keeping as much data as possible for the analysis.

Finally, it should be mentioned that the spatial resolution of the GNSS-R under coherent scattering regime is often associated to the size of the first Fresnel zone ($\sim$1 km from spaceborne platforms), although the incoherent averaging can downgrade it to a few km [24], [35] and the higher order Fresnel zones also contribute to the signal [36], [37]. Given the altitude of the considered satellites and their incoherent averaging time lapse of 1 s, the lower limit of the along track spatial resolution can be assumed about 6–7 km. The upper limit associated to an incoherent signal depends on the delay/Doppler discrimination and it is in the order of 25 km.

B. Test Areas

Five test areas were selected in the framework of this study (Table I). The areas were identified as examples of the most important forest types, and they included approximately the same range of biomass considered in the global analysis (i.e., $0 \leq AGB \leq 500$ t/ha). Since the low inclination angle of the CyGNSS satellite orbits does not enable the coverage of most of those areas, the local scale investigation was limited to the TDS-1 near polar orbiting satellite.

Extension and coordinates of each area were selected to match the frame of the available ALOS images, to allow the comparison with the ALOS data. In particular, the areas have an extension of approximately 350 km x 350 km, according to the Scansar ALOS

acquisition mode, except Uruguay, for which smaller Stripmap images (70 km x 70 km) were only available.

C. TechDemoSat-1 Data

TDS-1 is a U.K.-funded technology demonstrator mission built and launched by SSTL on July 2014 [11]. It carries on board, among others, the SGR-ReSI (Space GNSS Receiver Remote Sensing Instrument), collecting the GPS reflections and delivering the DDM's. The satellite flies at an altitude of 635 km and in a near-polar orbit, being the inclination of the orbital plane $\simeq 98°$.

TDS-1 data from July 2016 to September 2017 have been considered. For each of the test areas listed in Table I, all TDS-1 acquisitions in a $+/-15$ days window centered on the ALOS acquisition time (see following Section E) were extracted on the same area covered by ALOS. Because of the poor TDS-1 coverage of the areas, such temporal window was set as a compromise between the need of increasing the amount of TDS-1 data for the comparison, and the need of mitigating the effect of changes that can occur in the observed areas between the ALOS and TDS-1 acquisitions. In particular, such range was set to provide at least 200 reflectivity values at each date. The slow dynamics of forest biomass, especially in equatorial forests, helped in keeping these constraints.

All the variables required in (1) and (2) and the SNR have been derived from the original L1b daily TDS-1 product. The L1b data are made available by SSTL through the Merrbys portal (http://merrbys.co.uk/), under a Creative Commons Attribution, Non Commercial 4.0 International License. Data have been screened using the provided quality flags (satellite in eclipse and direct signal in the DDM). More information on the original format can be found in the Data Handbook available at the Merrbys website.

D. CyGNSS Data

The CyGNSS NASA mission, led by the University of Michigan in Ann Arbor, uses eight microsatellites, with a GNSS-R payload on board developed by SSTL, collecting GPS reflections to measure wind speeds over the Earth's oceans [12]. The eight microsatellites orbit at an inclination of 35°, and are each capable of measuring four simultaneous reflections, resulting in 32 wind measurements per second across the globe. CyGNSS data collected over land on a global scale within a latitudinal range of approximately $+/-38°$ have been downloaded from the Physical Oceanography Distributed Active Archive Center (https://podaac.jpl.nasa.gov). In particular, the Level 1b (version 2.1) data in NetCDF format have been considered for the period April–September 2017. NetCDF daily files, one for each CyGNSS observatory, contain the DDMs of analog scattered power for each SP, along with a number of useful metadata expressing the geometry of the acquisitions and information about the transmitting GPS satellite and the CyGNSS observatory receiving the reflection. Data were screened using the land flag, plus an "overall quality flag" included in the dataset [38]. The equivalent reflectivity $\Gamma(\theta)$ was computed according to (1) and regridded on the coordinates of the reference data considered

TABLE II
OVERVIEW OF ALOS IMAGES USED IN THIS STUDY

Area	N. of images	Date of first image acquired	Date of last image acquired
Alaska	9	24/07/2016	23/07/2017
Finland	5	07/01/2017	10/06/2017
Manaus	15	18/07/2016	17/07/2017
Argentina	10	22/07/2016	21/07/2017
Uruguay	4	04/10/2016	29/07/2017

in the various comparisons. The main difference with respect to TDS-1 is the use of the EIRP value provided in the L1b product rather than exploiting the direct signal power [11]. Because of its low inclination orbit (35° as specified above), CyGNSS does not cover the northern areas and it was mainly considered for the global scale analysis.

E. ALOS-2 Data

Time series of ALOS-2 images were collected on the test areas to supply another proxy of forest biomass and also to evaluate GNSS-R in comparison to monostatic radar observations of forests. Images were collected between 2016 and 2017, in order to have data representative of the whole yearly cycle. Most of the available ALOS images are in dual polarization (HH/HV) Scansar mode, with the exception of the Uruguay area where available data are in Stripmap mode and one acquisition is in quad-pol. Table II summarizes the number of images available for each area and the respective time frame. It should be noticed that, after a preliminary analysis, only summer images have been considered for Finland and Alaska, in order to avoid influence of snow cover and thaw/freezing processes. The images were radiometrically calibrated and geocoded by using orbital parameters and calibration coefficients provided along with each image. Geocoding was based on the Shuttle Radar Topography Mission digital elevation model (SRTM-DEM). The images were multilooked and coregistered in a stack file to allow multitemporal and multipolarization comparison pixel-by-pixel. Outputs of this processing were the calibrated backscattering coefficients ($\sigma°$) in HH and HV polarizations at 100-m resolution. For the comparison with TDS-1, these $\sigma°$ values have been averaged on a window centered in each TDS-1 acquisition (see following Section III-A).

F. SMAP VOD

The SMAP data considered for the scopes of this study were the L3 v.5 Radiometer global daily Equal-Area Scalable Earth Grid (EASE-Grid) data, with a spatial resolution of 36 km $\times$ 36 km [26]. Besides soil moisture, quality flags, and other auxiliary information gridded over the EASE-Grid v2.0, the VOD is available in the files. According to the SMAP documentation, the VOD considered here is returned by the processing software, when the Dual Channel Algorithm is used (L2 SM option 3). According to [39], VOD is the "tau" parameter which, after normalization by the cosine of the incidence angle, is used in the "tau-omega" model [40] for computing the transmissivity T

Dataset	Spatial Resolution
TDS-1	$\geq$ 7x1 Km^2
CyGNSS	$\geq$ 7x1 Km^2
ALOS	$\simeq$ 100 x 100 m^2
SMAP VOD	36 x 36 Km^2
AGB pantropical map	1x1 Km^2 (resampled at 5x5 Km^2)
ICE-GLAS tree height map	1x1 Km^2 (resampled at 5x5 Km^2)

of vegetation canopy:

$$T = e^{-\frac{\tau}{\cos(\theta)}} \tag{3}$$

where θ is the observation (incidence) angle, and τ is often parameterized as the product of a vegetation-type dependent b factor and the vegetation water content. VOD data have been extracted on the test areas indicated in Table I, at the same dates of ALOS images summarized in Table II.

G. AGB Map

The improved pantropical biomass map proposed in [27] was selected as reference for AGB for the scopes of this study. The map contains global AGB values in t/ha, at a resolution of 1 km. The map is limited to $+/-40°$ of latitude, thus hampering the comparison on boreal forests. It has been realized by applying a data fusion approach over two preexisting datasets of AGB and an independent field observations dataset [41], [42].

It should be mentioned that, to compare acquisitions of both TDS-1 and CyGNSS against a "static" reference AGB, the time series of satellite acquisitions aggregated at each point of the grid have been averaged as reported in Section III-C, thus losing the sensitivity to the variations of soil moisture and other surface features that affect the signal dynamics.

H. Tree Height Map

As a further comparison, a global map of tree height derived from ICE-GLAS LiDAR acquisitions as in [28] was also considered. The map provides tree height values in meters at 1-km resolution on a global scale. The GLAS canopy height is estimated as the distance between signal beginning and the location of the Lidar ground peak. The map was extended to areas not directly covered by the Lidar footprints by using the Random Forest algorithm [43], including vegetation information from MODIS, additional elevation data from the SRTM-DEM, and climatology information from both the Tropical Rainfall Measuring Mission and the Worldclim database. As for the AGB map, the possible time mismatch between this reference dataset and the GNSS-R data can affect the comparison.

To summarize, the spatial resolution of the data considered in this analysis is listed in Table III. For the comparison with VOD, the GNSS-R data from both TDS-1 and CyGNSS, and the ALOS PALSAR data were aggregated at a resolution of 36 x 36 Km^2 to match the SMAP EASE-Grid. For the comparison and the retrievals of AGB and H, all data (GNSS-R and reference maps) were aggregated at 5×5 Km^2. The time period investigated
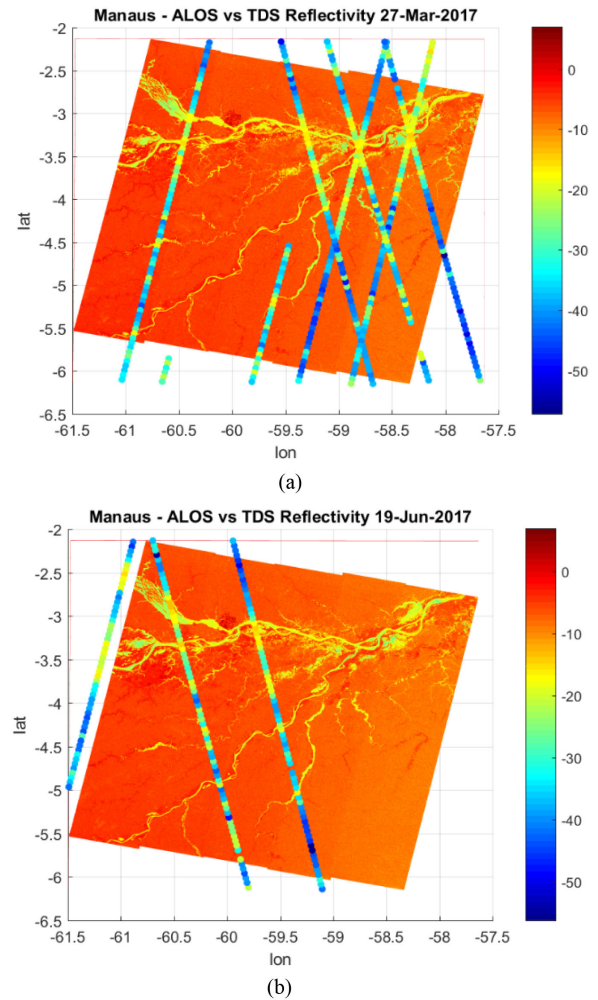

Fig. 1. Examples of ALOS $\sigma°$ and TDS-1 Γ overlapped acquisitions on the Manaus area. (a) ALOS acquisition of 27 March 2017. (b) ALOS acquisition of 19 June 2017. Colors are proportional to the signal ($\sigma°$ and Γ), according to the colorbar.

in this study was the one covered by ALOS in the comparison between ALOS and TDS-1 (Table II) and the common period between TDS-1 and CyGNSS (April to September 2017) for the remaining comparisons.

III. SENSITIVITY ANALYSIS

A. Local Comparison Between ALOS and TDS-1

We recall that monostatic and specular scattering mechanisms show opposite sensitivity to biomass. Backscatter increases with biomass because of the greater volume scattering, eventually reaching saturation because of the simultaneous increasing attenuation, whereas specular reflection decreases monotonically as a consequence of the increasing attenuation. This opposite behavior of monostatic and specular mechanisms is evident from the two maps of $\sigma°$ and Γ for the Manaus area represented as examples in Fig. 1. The maps show clearly that $\sigma°$ has the highest values on dense forests and lowest values on open water. As expected, the overlapped tracks of Γ along the TDS-1 orbit has
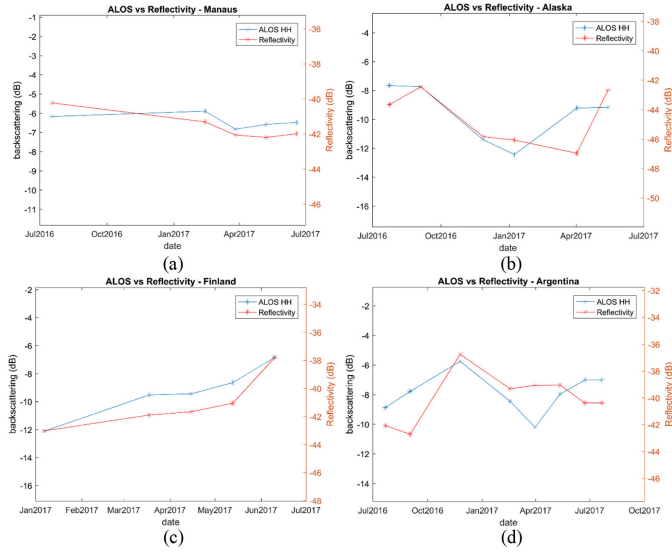
Fig. 2.   Temporal trends of ALOS and TDS-1 acquisitions computed for the period June 2016–July 2017. (a) ALOS σ° in HH pol. and TDS-1 Γ on the Manaus test area. b) Same for Alaska, (c) for Finland, and (d) for Argentina.

TABLE IV
CORRELATION COEFFICIENTS OF THE RELATIONSHIP Γ VS. VOD

area	R	n. of samples	VOD range
Alaska	-0.11	1031	$0.7 - 1.0$
Finland	-0.39	945	$0.1 - 0.8$
Manaus	-0.61	3182	$0.2 - 1.4$
Argentina	-0.44	3316	$0.2 - 1.0$
Uruguay	-0.61	401	$0.3 - 1.2$

opposite behavior, i.e., low values on dense forests, high values on open water. Despite the contribution from both specular and diffuse components, the attenuation of the former shows to be a relevant mechanism.

The temporal trends of TDS-1 reflectivity and ALOS σ° on the considered areas were then analyzed. For this scope, the data were filtered for presence of open water, urban areas, and not forested areas. Filtering was based on GlobCover Land Cover maps [44]. Then, some homogeneous subareas of each test area were identified, on which the variation of both Γ and σ° were within a range of ± 1 dB. This was done to mitigate possible errors depending on colocation and different spatial resolution between the two sensors. On these subareas, ALOS pixels were averaged on a 5 Km $\times$ 5 Km window centered on each TDS-1 SP, in order to approximately match the expected TDS-1 spatial resolution. We reassert that, due to the $+/-15$ days window, single pass ALOS acquisitions were compared with one month of TDS-1 data.

A few examples of the observed temporal trends are displayed in Fig. 2.

The plot in Fig. 2(a), referring to the Manaus test area, confirms the high and constant values of ALOS σ° (around $-6/-7$ dB) over the dense forests that cover the region. Γ exhibits almost comparable stable values in both space and time.

On the Alaska test area [Fig. 2(b)]], ALOS σ° exhibits a seasonal cycle, which is followed by Γ as well. The information on snow presence, derived from the AMSR-E/AMSR2 Level-3 daily Snow Water Equivalent maps [45], confirmed that the lower Γ values found during the winter season depend on snow presence and on the frozen conditions of soil and plants that have a significant influence on the TDS-1 measurements. Therefore, the data collected in winter have been excluded, before attempting a direct evaluation of the TDS-1 sensitivity to the forest biomass. From the plots, a delay in the increase of

TDS-1 observables with respect to ALOS σ° (in April 2017) can be possibly attributed to the TDS-1 earlier acquisition date.

The analysis of temporal trends for the Finland test area [Fig. 2(c)] confirms the signal behaviors shown in the Alaska area, although in this case, ALOS data were available only from January 2017, thus limiting the analysis to the second part of the winter season.

In Argentina [Fig. 2(d)], σ° shows a clear seasonal cycle, with high values in November and low values in April, which is also observed in the Γ plot. Based on the few information available, mainly represented by the antecedent precipitation index derived from the meteorological stations, this behavior can be attributed to soil moisture, which in November is expected to be higher than in April [46]. Unfortunately, reference soil moisture data to support this assumption were not available.

Finally, on the dense coniferous area of Uruguay (not reported in Fig. 2 for brevity), both σ° and Γ exhibited almost constant values. It should be however mentioned that, depending on the poor TDS-1 coverage of the area, the overlap of TDS-1 and ALOS is limited to two of the four dates available in Uruguay.

B. Comparison of GNSS-R With VOD From SMAP

In this section, Γ derived from both spaceborne GNSS-R instruments is compared to SMAP VOD on local and global scale.

The Γ values derived from the daily TDS-1 acquisitions over the test areas were compared with the VOD data acquired at the same dates: For this scope, TDS-1 data were averaged within each cell of the SMAP grid. The analysis also included the σ° extracted from the available ALOS images.

The correlation coefficients between Γ and VOD for each area are reported in Table IV, along with the number of samples and the VOD range.

In all areas, Γ decreases when VOD increases. Alaska and Finland exhibit the worse correlations, depending on some residual snow and soil thawing/refreezing effects that the masking based on the AMSR2 SWE maps was not able to remove completely.

The scatterplot of TDS-1 vs. VOD combining all the available data in the selected areas is displayed in Fig. 3(a). The correlation coefficient is $R = -0.54$ and the sensitivity is about 16 dB per VOD unit. As a term of comparison, the corresponding scatterplots of ALOS σ° in HV polarization as a function of VOD is shown in Fig. 3(b).
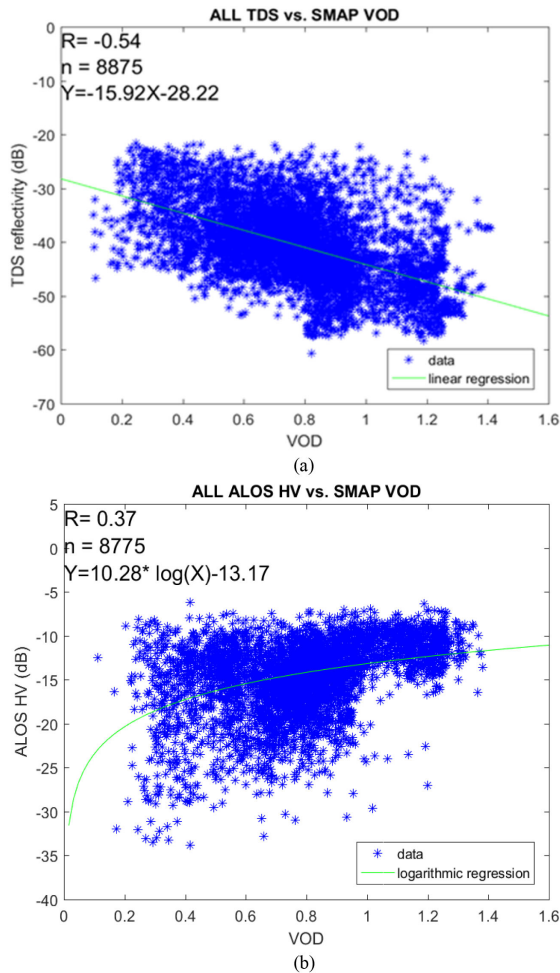
Fig. 3. Scatterplot between (a) TDS-1 Γ and (b) the ALOS σ° HV as a function of the VOD at 36 km resolution (SMAP L2 product). Green lines represent the best fitting.

Fig. 4. CyGNSS Γ plotted as function of VOD on a global scale. Color scale indicates the density of points.

The comparison of scatterplots in Fig. 3(a) and (b) well point out that, although both ALOS and TDS-1 operate at L-band, σ° is less correlated to VOD ($R = 0.37$) than Γ, and it exhibits a clear saturation effect for higher VOD values, while reflectivity decreases almost linearly. The ALOS backscattering shows an overall dynamic range of less than 10 dB/VOD unit, in the range of VOD between 0.2 and 1.

The analysis was extended to global scale by using CyGNSS: The daily Γ values were aggregated on the SMAP grid and compared to the SMAP VOD. The density plot of Fig. 4 shows the decreasing trend of Γ from CyGNSS when VOD increases, although with rather low correlation coefficient $R = -0.33$. The regression equation shows a sensitivity of about -7 dB per VOD unit, that is lower than the one obtained from the local analysis using TDS-1. Besides the differences in the calibration procedure between TDS-1 and CyGNSS, other factors concur to this result, including the effect of the variability of other surface parameters that is larger at global than at local scale, and disturbance due to the inclusion of nonforested area with VOD > 0.

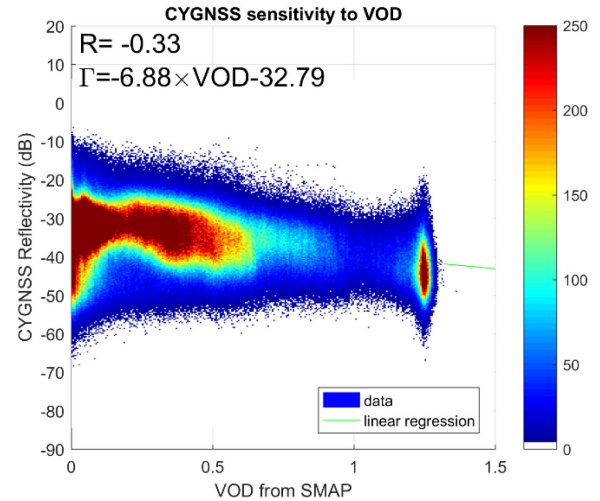The results shown in this section confirm an encouraging Γ sensitivity to VOD, as already pointed out in [21], and arguably, to any other parameter directly related to the forest biomass. Indeed, although VOD is not a vegetation variable but an electromagnetic parameter, it is related to the vegetation biomass [47]. Furthermore, it is the only parameter available on a global scale and with frequent revisiting, provided by SMAP and by Soil Moisture Ocean Salinity, the other satellite carrying on board an L-band radiometer. Therefore, it represents the only proxy of the biomass parameter available with global coverage and daily revisiting.

To further assess these results, the sensitivity analysis included the AGB pantropical and the global ICE-GLAS H maps, both available at global scale and with a resolution suitable for the comparison with TDS-1 and CyGNSS. The main limitation is that both AGB and H are provided as "static" maps, i.e., as single values that are accurate for forest conditions prior to GNSS-R acquisitions. Since those datasets are not available as time series, the Γ values at each point of the spatial grid have been temporally averaged, with the positive effect of weakening any sensitivity to other soil parameters that disturb the retrieval of biomass.

C. Comparison of GNSS-R With Pantropical AGB Map

The TDS-1 and CyGNSS sensitivities to AGB were evaluated by comparing Γ to the improved pantropical biomass map.

The comparison on a local scale was carried out on the common dataset, i.e., the month of April plus the period from July to November 2017, for the Argentina, Manaus, and Uruguay test areas. Since the AGB map is limited to $+/-40^\circ$ latitude range, the boreal forests are excluded, while the data from the remaining areas were combined for this comparison.

In this case, it makes sense considering in the local comparison CyGNSS as well, having similar latitude bounds as the AGB map. Γ derived from both TDS-1 and CyGNSS, as well as AGB and ALOS backscatter, were resampled on the grid of the AGB

TABLE V
MAIN STATISTICS OF THE RELATIONSHIP Γ VS. AGB

area	R	slope	n. of samples	AGB range
Alaska			no AGB data	
Finland			no AGB data	
Manaus	-0.36	-0.05	1067	5 - 370
Argentina	-0.15	-0.01	243	5 - 70
Uruguay	-0.32	-0.02	144	30 - 140

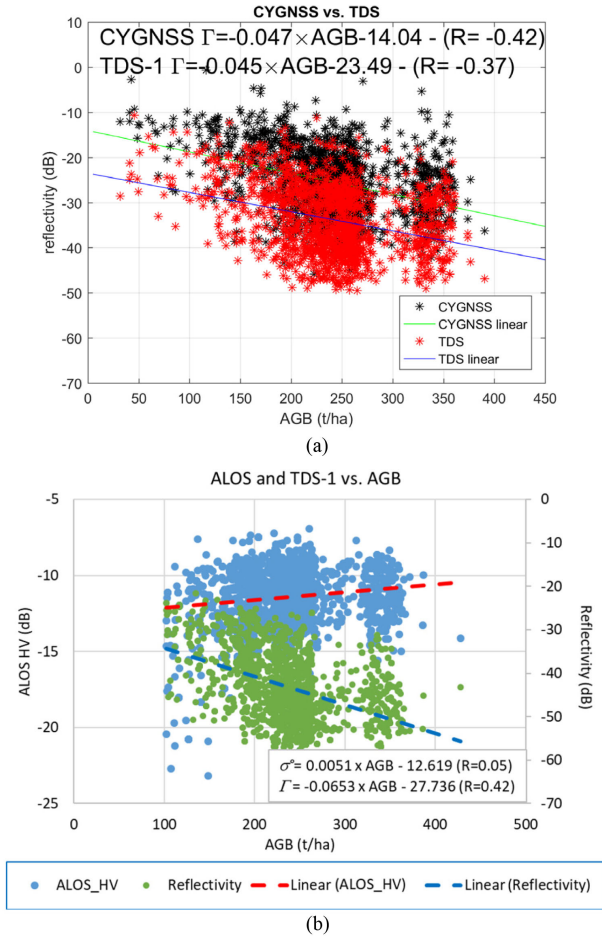Fig. 6. CyGNSS Γ plotted as function of AGB on a global scale.

Fig. 5. (a) TDS-1 and CyGNSS Γ vs. AGB from pantropical map for the Manaus, Argentina, and Uruguay test areas: the regression equations and corresponding correlation coefficients are provided in the plots. (b) ALOS backscatter and TDS-1 reflectivity as a function of AGB for biomass values higher than 150 t/ha.

map (5×5 Km^2), by averaging all the values in the same cell of the grid.

The main statistics of the analysis are summarized in Table V.

Table V shows slightly worse correlations with respect to the comparison with VOD (Table IV), depending on the above-mentioned limits of this comparison. Also, the smaller range of AGB and number of samples for Uruguay and Argentina had effect on the correlation.

The scatterplot of Γ from both CyGNSS and TDS-1 as a function of AGB obtained by grouping the data from the selected three areas is shown in Fig. 5: Despite the aforementioned limitations
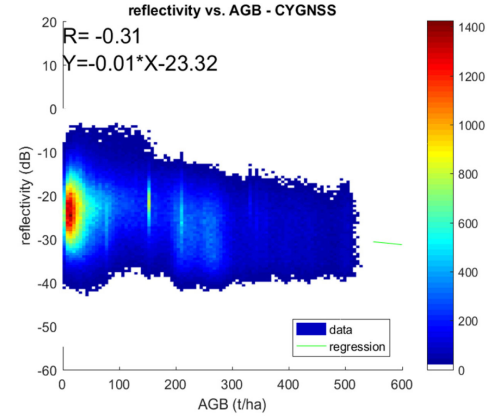
inherent the "static" AGB map, the results shown in Fig. 5(a) can be considered encouraging. The different approach followed to compute Γ, depending on the different parameters available in the L1b data files, leads to an offset between CyGNSS and TDS-1 data that can be observed in Fig. 5(a). However, the slope of both regressions is almost the same [0.047 dB(t/ha)$^{-1}$ for CyGNSS and 0.045 dB(t/ha)$^{-1}$ for TDS-1]. The two regression equations are indeed $\Gamma = -0.047 \times$ AGB-14.04 for CyGNSS and $\Gamma = -0.045 \times$ AGB-23.49 for TDS-1. The same happens for the correlation coefficient that is $R \simeq 0.4$ in both cases. Note that the absolute calibration is a well-known issue for spaceborne GNSS-R, but it does not affect too much the data-driven approach proposed in the sequel for retrieval, provided the training is carried out independently for the two instruments.

Then, the backscattering coefficient $\sigma°$ derived from the ALOS images has been also considered. The scatterplot of ALOS $\sigma°$ in HV polarization and TDS-1 Γ, plotted as a function of AGB in the range 100–400 t/ha, is shown in Fig. 5(b). The value of 100 t/ha represents the saturation threshold for L-band SAR, as evaluated, e.g., in [20]. The plot confirms the almost complete saturation of $\sigma°$ for AGB higher than 150 t/ha, while Γ is decreasing almost linearly down to the maximum AGB available in the dataset. The obtained sensitivities confirmed the simulation analysis of specular versus backscatter observations [15], [16], and the experimental results obtained from low platforms GNSS-R experiments [17], [18].

The comparison between Γ and AGB was extended to a global scale, although limited to the $+/-40°$ latitude bound, considering CyGNSS. For this scope, the timeseries of CyGNSS data aggregated on each point of the coordinates grid of the AGB pantropical map (5×5 Km^2) were averaged on the entire period, as done for TDS-1. The comparison was carried out for all the valid values in the AGB map that already accounts for open waters, deserts, and urbanization. The result is shown in the density plot of Fig. 6. The correlation was lower ($R = -0.31$), but the decreasing trend with increasing biomass shown in Fig. 5(a) is confirmed. The high scatter of the plot may depend again on the single reference AGB considered, especially in the case of sparse forests, for which the temporal variability of soil moisture and roughness affect the most the signal.

area	R	slope	n. pixels	*H* range (m)
Manaus	-0.49	-0.83	1114	11-37
Uruguay	-0.39	-0.25	157	6-25
Argentina	-0.30	-0.12	191	7-12
Alaska	-0.15	0.09	231	8-26
Finland	-0.33	-0.23	327	9-23

D. Comparison of GNSS-R With ICE-GLAS Tree Heights

The ICE-GLAS tree height map (H) was finally considered for assessing the GNSS-R sensitivity to the forest biomass. The correlation between tree height and biomass is indeed generally high for a single species.

As in the case of AGB, the comparison between Γ and H has been carried out at local scale by using TDS-1 data, and then extended to global scale by using CyGNSS, since the latter satellites do not cover some of the test areas, depending on the already mentioned low inclination orbit.

The results of the sensitivity analysis carried out area by area using TDS-1 are summarized in Table VI.

The results in Table VI reflect those in Table V and similar considerations can be done. The best sensitivity is again exhibited by the Manaus area, taking advantage of the largest H range and of the better coverage, while R decreases in Uruguay, also depending on the smaller size of the area, and in Argentina, depending on the mixed vegetation cover, as evidenced by the lowest H values.

Both TDS-1 and CyGNSS data were averaged and aggregated on the coordinates grid of the H map (5×5 Km^2), as done for the AGB pantropical map. In this case too, all the valid data in the H map have been considered for the comparison.

The "local" scatterplot of TDS-1 vs. H, obtained by grouping the data on all the test areas, is shown in Fig. 7(a): Γ shows an almost linear decrease when the height of trees increases, with $R \simeq -0.4$ and sensitivity is about -0.66 dB/m. The result is confirmed at global scale using CyGNSS, although with higher dispersion of data [Fig. 7(b)]. In this case $R \simeq -0.36$ and sensitivity is -0.23 dB/m.

The presence of many different forest types in the global analysis may contribute to increase the dispersion, being the relationship H vs. biomass dependent on the tree species. Moreover, the dispersion also depends on the temporal variability of other surface parameters that has not been accounted for.

IV. BIOMASS RETRIEVAL

The results shown in the previous section pointed out a negative correlation between the equivalent Earth's surface reflectivity and the different parameters associated to the volume of plants (biomass and height), as well as their electromagnetic extinction properties (VOD). These results confirm what was predicted by electromagnetic models for GNSS-R specular observations. The DDM peak is a combination of specular and
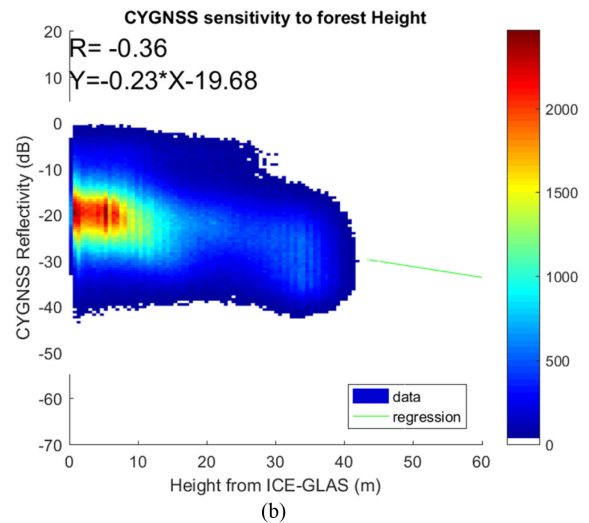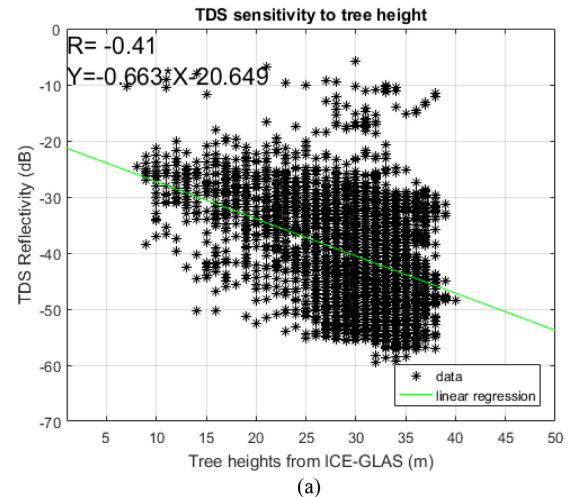

Fig. 7. Γ as a function of tree height estimated by the ICE-GLAS mission. (a) TDS-1 over the test areas. (b) CyGNSS on a global scale.

diffuse scattered signals; however, the negative correlation is mainly determined by the specular reflection from the soil which is attenuated by the vegetation [15]. It also confirms the outcome of previous studies mentioned in the introduction.

Despite the high scatter of the experimental points, a preliminary investigation of the GNSS-R capabilities in estimating the forest biomass was carried out. When possible, ancillary data were introduced in the retrieval algorithm to mitigate the ill-posedness of the inverse problem. Prototype retrieval algorithms based on ANN were developed, with the aim of estimating AGB and forest height from Γ derived from TDS-1 and CyGNSS alone and in synergy with ALOS data. Algorithms were applied to local retrievals on the selected test areas and also globally.

A. ANN Retrieval Approach

Due to their ability in approximating almost any kind of nonlinear relationships [48], [49], the ANN is gaining an

ever-increasing attention for solving a wide variety of problems. In particular, ANN was largely applied to solve remote sensing problems, taking also advantage of the possibility to combine multiple sources of information into the same retrieval algorithm (e.g., [50]–[54]).

For this preliminary investigation, the feed-forward multilayer perceptron neural networks (MLP-ANN) available in the Matlab Neural Networks toolbox were considered. The MLP-ANN training was based on the back propagation learning rule. The scheme of this implementation followed the strategy presented in [55].

B. ANN Architecture Definition and Training

The data considered for training, validating, and testing the algorithm were derived from the overall database of TDS-1 and CyGNSS observables combined with the corresponding vegetation parameters (biomass, or height, depending on the considered reference set) and possibly $\sigma°$ measurements by ALOS-2. In details, from each of the available dataset presented in Section II, a subset of data was considered for training the algorithm and the remaining data for testing its performance, by predicting biomass and height from a set of satellite data not considered in the training phase. The percentage of the entire data set used as *training* and *test subsets* ranged from 50% and 50% for the retrieval experiments on a local scale to 1% and 99% for the experiments on a global scale.

The generation of training and test sets is summarized in the flowchart of Fig. 8: According to the workflow, the *training* set was further subsampled randomly in 60%, 20%, and 20% subsets, for having the ANN training and a posteriori "test" and "validation" at each training iteration.

Such strategy can be considered sufficient for validating the algorithm, however, in an attempt of keeping training and test as independent as possible, we preferred to test the ANN on a dataset (i.e., the second subset of the entire set, denoted as *test subset*) not involved in the training.

The optimal ANN for the given problem was defined by increasing iteratively the ANN configuration from one hidden layer with a number of neurons equal to the number of inputs, up to two hidden layers with a number of neurons each equal to three times the number of inputs. This process was iterated for each transfer function available, among linear, tansig, and logsig.

The "optimal" ANN was composed of two hidden layers with a number of neurons varying between 7 and 10, with transfer function of type tansig or logsig, depending on the considered case (retrieval of AGB or H, using TDS-1 or using CyGNSS). An example of ANN is shown in Fig. 8(b).

C. ANN Algorithm for Estimating AGB and Tree Height

Two retrieval exercises were conducted on a local scale using TDS-1 data. Algorithm inputs were Γ, the incidence angle, and the SNR. Although the latter parameter was found scarcely related to the forest biomass, including it as additional input
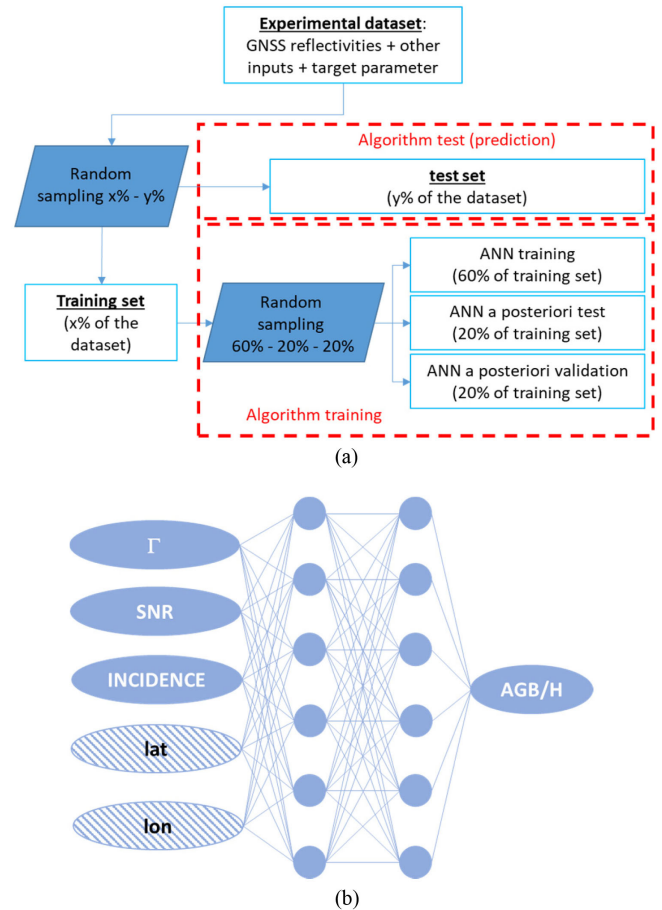

Fig. 8. (a) Work flow of the generation of training and test datasets. (b) Example of ANN scheme.

allowed slightly improving the retrieval. In both cases, 50% of the dataset was considered for training the ANN, and the remaining for testing the algorithm. The test results are shown in Fig. 9(a) for AGB and Fig. 9(b) for tree height (H). The test sets were composed of $n \simeq 9900$ and $n \simeq 10500$ samples, respectively, as indicated in the plots.

Although it should be reminded again that the "static" maps (AGB or H) are not the optimal references for comparing time series of satellite acquisitions, the obtained results are encouraging, as pointed out by $R \simeq 0.8$ obtained in both cases, and RMSE of 38 t/ha for AGB retrieval (in the range 100–400 t/ha) and 3.1 m for H retrieval (in the range 10–40 m), respectively. The retrieval was then extended to a global scale by setting up a new ANN using CyGNSS data. Depending on the different level of Γ, the training has been repeated by considering 1% and 99% of data for training and test, respectively. In the global case, the geographic position of each pixel was added to the ANN inputs, leading to a (slight) improvement of the retrieval. The test set was composed in both cases of about 1.5 million of samples.

The retrieval results are shown in Fig. 10, where the AGB [Fig. 10(a)] and H [Fig. 10(b)] estimated by the ANN by using
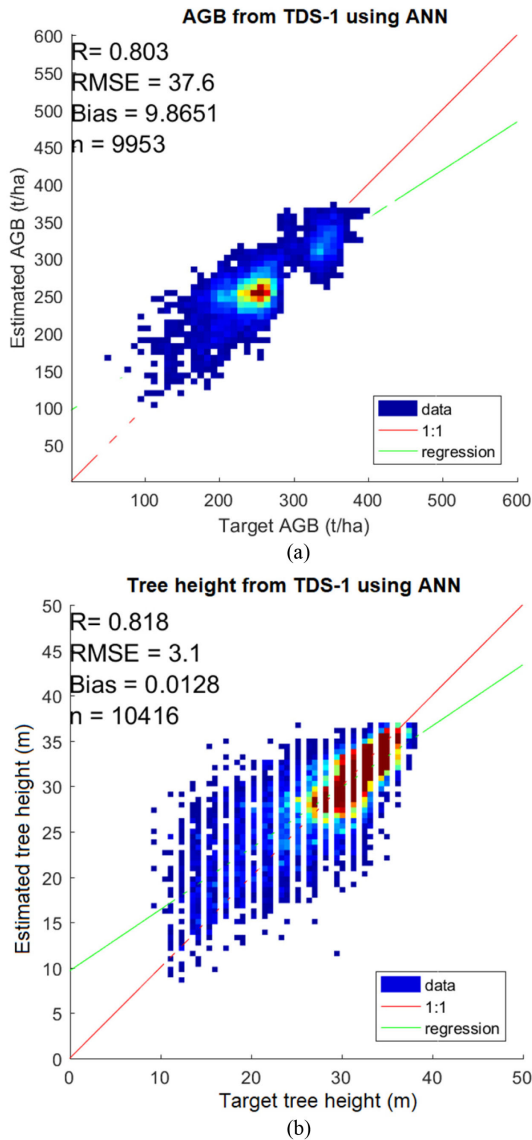
Fig. 9. AGB and *H* retrieval on the test areas using TDS-1 data. Density plot of (a) estimated vs. target AGB, (b) estimated vs. target tree height.

Fig. 10. AGB and *H* retrieval on a global scale using CyGNSS data. (a) AGB estimated by ANN as a function of the reference from the pantropical map. (b) Tree height estimated by ANN as a function of the reference *H* from the ICE-GLAS data.

CyGNSS data are represented as a function of the corresponding target parameter. The correlation coefficients of AGB and *H* retrieval are good, $R \simeq 0.82$ and $R \simeq 0.80$, respectively, and the RMSE slightly worse than on the local scale, i.e., 76 t/ha for AGB retrieval (in the range 100 to 500 t/ha) and 6.5 m for *H* (in the range 0–40 m).

D. Local and Global Biomass Maps

Based on these results, maps of the estimated parameters were generated from TDS-1 and CyGNSS over the considered areas. As an example, the maps of AGB and tree height derived from TDS-1 for the area of Manaus are shown in Fig. 11 in comparison with the pantropical AGB and Lidar *H* maps, respectively. Absolute difference maps between estimated and target quantities are also shown. Manaus was selected as example based on the
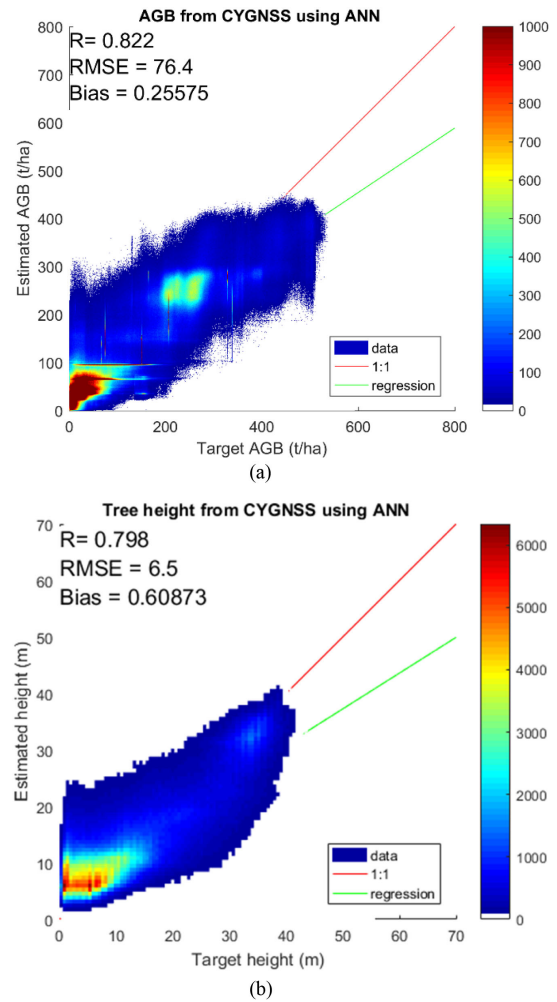
results in Tables IV–VI, since it covers a range of biomasses larger than the other areas and close to the global AGB range. To facilitate the comparison, the gaps of TDS-1 acquisitions are also reported in the reference maps. In both AGB and *H* retrievals, the behavior of the estimated parameters seems to follow the corresponding reference data and the patterns are correctly reproduced, although some smoothing of the highest values in the ANN map has to be pointed out, as it can be argued referring to the scatterplots in Fig. 10. This does not necessarily depend on TDS-1-related issues, since the tendency of ANN to overestimate the lower values and underestimate the higher ones has been already pointed out in other works (e.g., [51]). This can be explained considering that ANN is based on a minimization of the error variance and the training samples representative of the highest and lowest values of the target parameter are in general scarce.

The TDS-1 coverage appears the main limitation on the use of this technique for mapping forest biomass, since several gaps
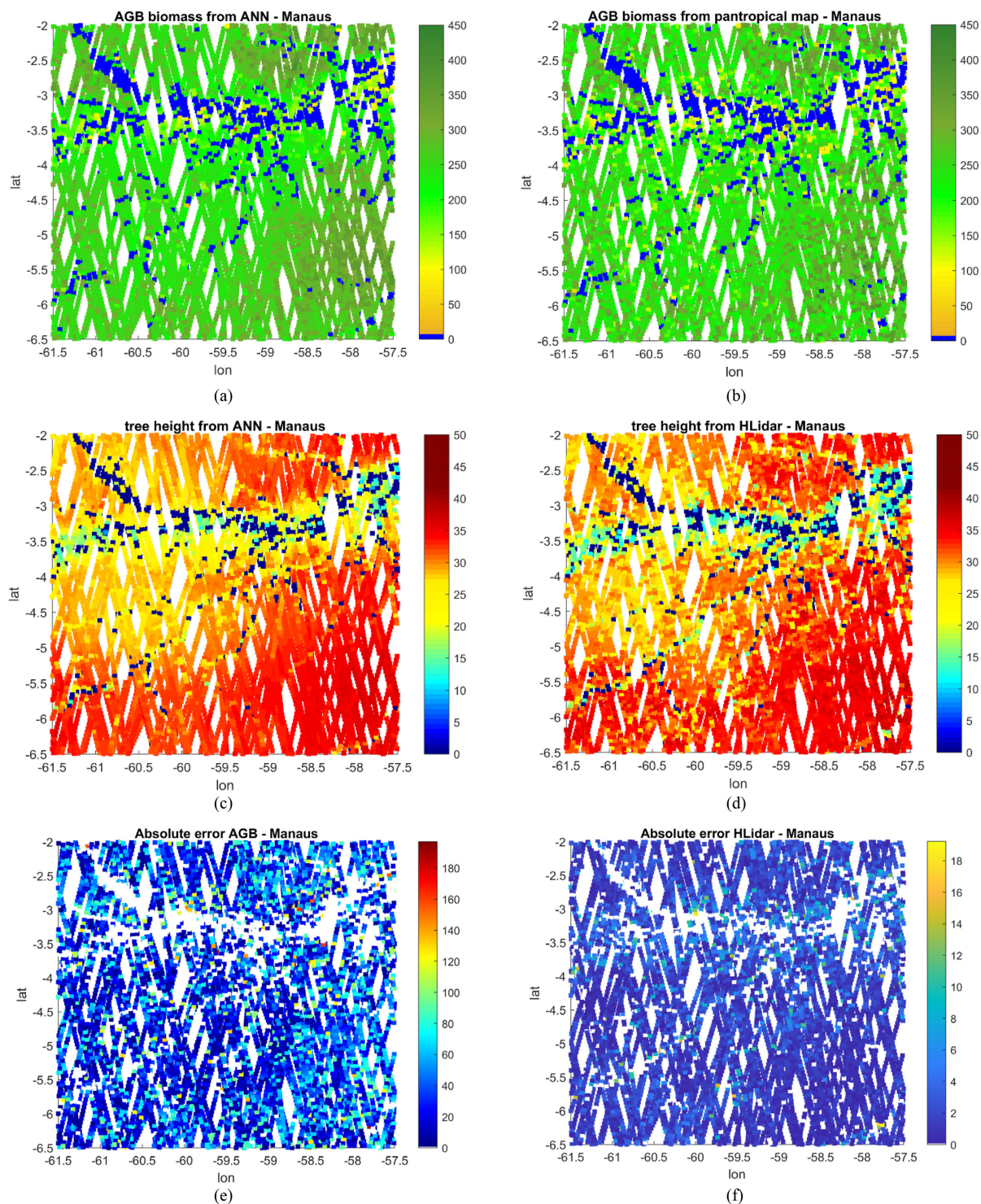
Fig. 11. Examples of maps of the target parameters. (a) AGB map generated by the ANN algorithm. (b) Corresponding reference from the pantropical map. (c) Tree height map generated by the ANN algorithm. (d) Corresponding reference from Lidar *H*. (e) Absolute difference between AGB estimated by ANN and target parameter. (f) Absolute difference between AGB estimated by ANN and target parameter. Note that the reference maps have been plotted only where TDS-1 reflections are, in order to better appreciate the differences.

due to missing TDS-1 data can be observed in the maps, despite the extended time interval considered. However, we remind that TDS-1 was a technological demonstrator that did not collect the data in a systematic way but during few days each month, with the exception of the last year of operation.

The AGB global biomass map generated by the ANN using CyGNSS data is shown in the upper panel of Fig. 12, while the corresponding target data from the pantropical map are shown in the mid panel. The agreement between the two maps is evident from the figures, and the corresponding statistics are in line with
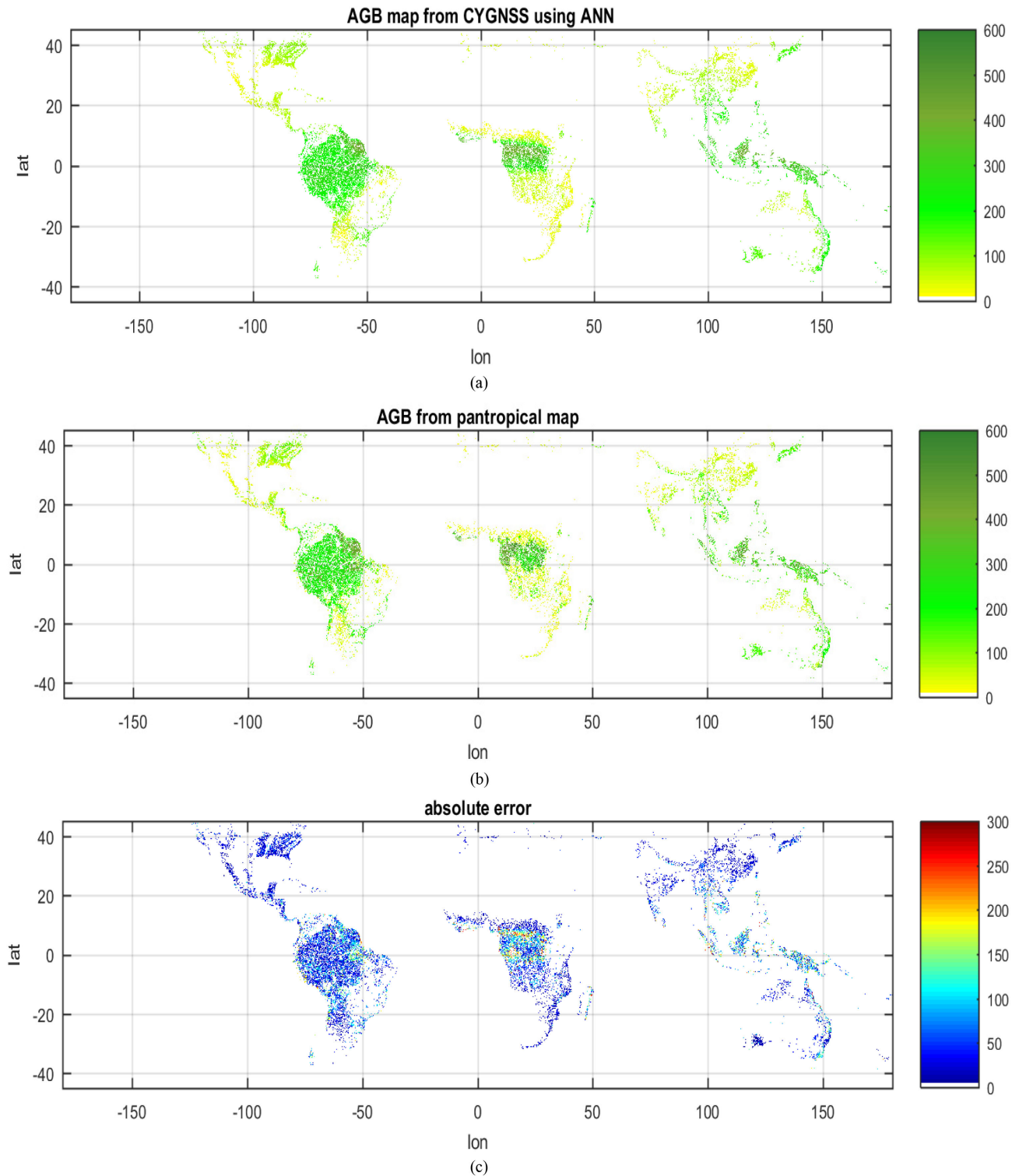
Fig. 12.   (a) AGB map generated by the ANN using CyGNSS. (b) Reference AGB from the pantropical map. (c) Absolute error map.

the results shown in Fig. 10(a). However, some local patterns with high biomass of the pantropical map are not correctly reproduced by the algorithm, as it can be deduced from the increase of the absolute error in some areas of equatorial forests in Africa and South America [Fig. 12(c)]. The underestimation of the AGB values higher than 400 t/ha was already observed in the scatterplot of Fig. 10(a), and it could be attributed either to the problem of considering a static map for the comparison or to the less dense training set over the highest biomass values.
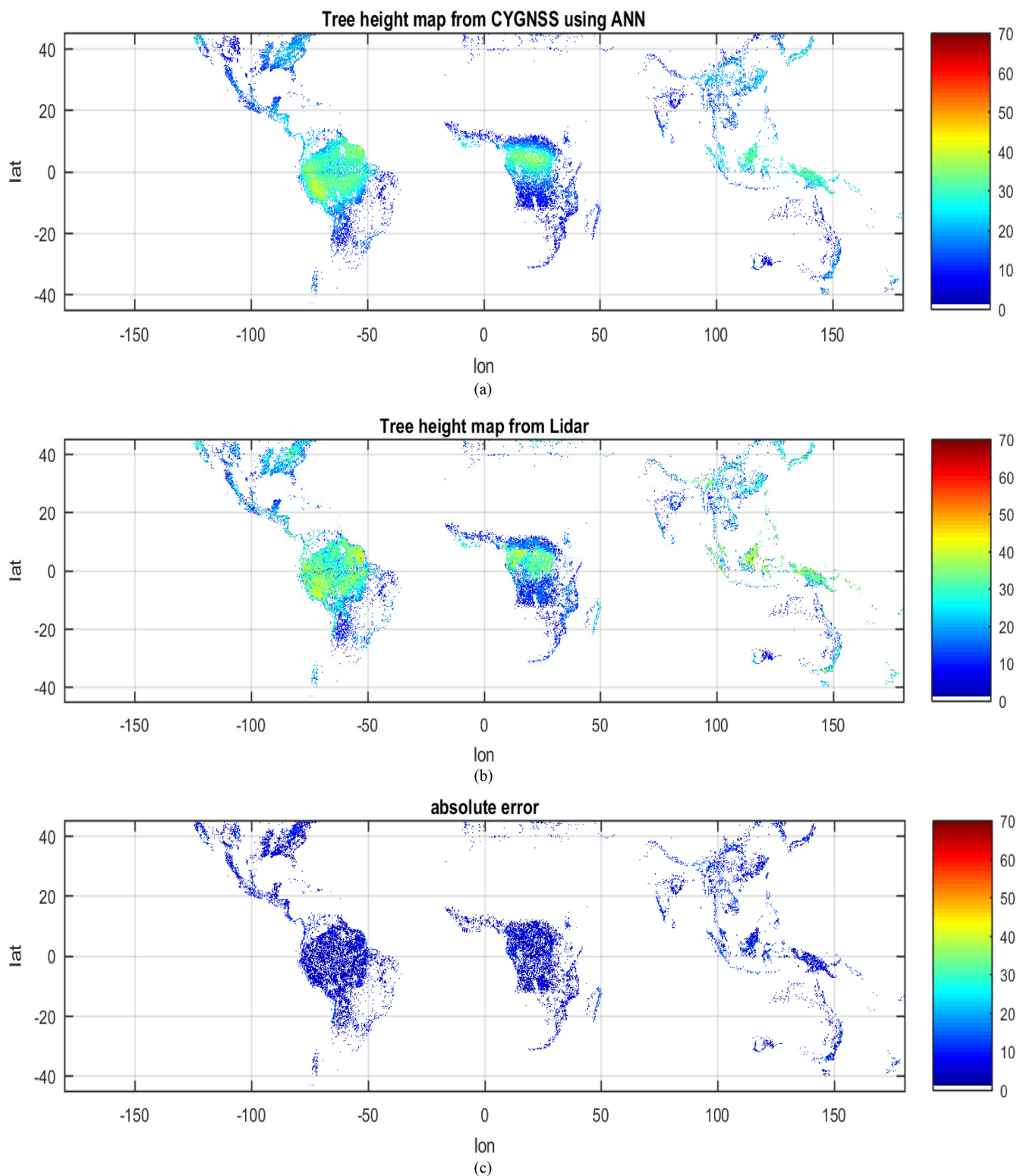
Fig. 13.   (a) Tree height map generated by the ANN using CyGNSS. (b) Reference height map from ICE-GLAS. c) Absolute error map.

As a final example, the tree height global map generated by ANN using CyGNSS and the reference map from Lidar H are represented in Fig. 13. The agreement between the maps is pointed out by the low values of absolute error, shown in Fig. 13(c).

V. CONCLUSION

In this research, the capability of GNSS reflectometry from space to retrieve forest biomass and other related parameters has been evaluated by analyzing data from the TDS-1 and the NASA

CyGNSS missions. An equivalent reflectivity (Γ) of the Earth's surface (e.g., soil plus vegetation) retrieved from the peak of the DDM was selected as the main observable for this application. It comprises both specular and diffuse scattering. Its sensitivity to forest parameters has been evaluated on a local scale, on five test areas selected as examples of the most important forest types and located in different parts of the Earth's surface, and then extended to a global scale.

Three different parameters related to forest biomass have been considered for this scope, all available on a global scale with different spatial resolution: the SMAP VOD, the improved pantropical AGB map, and the global map of tree height (H) derived from the ICE-GLAS satellite LiDAR.

As ancillary data, backscatter images from the ALOS-2 PAL-SAR L-band SAR have also been considered with the scope of comparing the GNSS-R performances with those of a monostatic radar. The sensitivity analysis, conducted on both local and global scales and considering both GNSS-R missions, confirmed the decreasing trend of the equivalent reflectivity when the target parameter related to the biomass, either VOD, AGB, or H, increases, with absolute value of the correlation coefficient in the range $0.3 \leq R \leq 0.54$. On a local scale, the corresponding sensitivities were 16 dB/VOD unit, 0.05 dB(t/ha)$^{-1}$, and 0.7 dBm^{-1}, for VOD, AGB, and H, respectively. The corresponding sensitivities at global scale were 7 dB/VOD, 0.01 dB(t/ha)$^{-1}$, and 0.23 dBm^{-1}. It should be mentioned that the sensitivity reported from two different airborne experiments was 0.015 dB(t/ha)$^{-1}$ and 0.05 dB(t/ha)$^{-1}$, respectively, thus the obtained results confirmed this range of values [18], [19]. The correlation coefficient is not very high, but we should consider the impact on the reflectivity of many other unknown factors (e.g., soil moisture and roughness) and of incoherent volume scattering, as well as the poor temporal matching among the data (despite the expected temporal stability of the forest conditions). It is noticeable that the higher correlation was observed with VOD at a local scale, implying a good time matching between SMAP and TDS-1 data.

In contrast, both AGB pantropical and ICE-GLAS H maps are generated using data older than the GNSS-R acquisitions. The slow forest dynamics should help in mitigating the differences, in any case, we can reasonably assume that the actual correlations can be higher than those found in this study.

The analysis also confirmed the better sensitivity of the GNSS-R technique with respect to an L-band radar, especially for the highest value of biomass.

The retrieval of the forest parameters has been implemented by ANN, using ancillary data, when possible. In particular, both SNR and incidence angle were found useful for improving the retrievals.

The test of the algorithms using a dataset independent of the training set resulted in a correlation coefficient $R \simeq 0.8$ between retrieved and reference quantities in the various experiments, and 37 t/ha $\leq$ RMSE $\leq$ 76 t/ha for local and global AGB retrievals (AGB in the range 0–400 t/ha), and 3.1 m $\leq$ RMSE $\leq$ 6.5 m for tree height retrieval (H in the range 0–45 m). Moreover, we can expect that these results would improve by considering

reference data with a better temporal matching to the GNSS-R acquisitions (when they will be available).

In conclusion, the sensitivity of GNSS-R data to forest parameters, related to the total biomass observed in previous works, was confirmed. The retrieval performances were also encouraging. As this is likely the first work attempting the retrieval of forest biomass on a global scale from satellite GNSS-R data, a more robust set of ground truth should be considered in the future, including up-to-date reference maps, for assessing the actual capability of GNSS-R in terms of spatial resolution. The use of ancillary information on other surface parameters, as the soil moisture, to improve the retrievals, as well as other observables derived from the DDM should be also investigated. More work should be finally devoted to exploiting the synergy of monostatic radar and GNSS-R.

As final remarks concerning the limitations of the current GNSS-R satellites, it should be recalled that TDS-1, being a technologic demonstrator, has a poor coverage (and moreover it ceased working few months ago), while CyGNSS is a constellation with better sampling, but it is limited to the central latitudes. The absolute calibration issue, the low power density impinging on the Earth's surface, and the high variability of the signal are other aspects that should be further investigated for a better exploitation of this technique over land.

References

[1] M. Martin-Neira, "A passive reflectometry and interferometry system (PARIS): Application to ocean altimetry," *Ecol. Soc. Amer. J.*, vol. 17, no. 4, pp. 331–355, 1993.

[2] V. Zavorotny, S. Gleason, E. Cardellach, and A. Camps, "Tutorial on remote sensing using GNSS bistatic radar of opportunity," *Geosci. Remote Sens. Mag.*, vol. 2, pp. 8–45, 2014, doi: 10.1109/MGRS.2014.2374220.

[3] N. Rodriguez-Alvarez, D. M. Akos, V. U. Zavorotny, J. A. Smith, A. Camps, and C. W. Fairall, "Airborne GNSS-R wind retrievals using delay–Doppler maps," *IEEE Trans. Geosci. Remote Sens.*, vol. 51, no. 1, pp. 626–641, Jan. 2013, doi: 10.1109/TGRS.2012.2196437.

[4] C. S. Ruf *et al.*, "A new paradigm in earth environmental monitoring with the CYGNSS small satellite constellation," *Sci. Rep.*, vol. 8, 2018, Art. no. 8782, doi: 10.1038/s41598-018-27127-4.

[5] C. C. Chew and E. E. Small, "Soil moisture sensing using spaceborne GNSS reflections: Comparison of CYGNSS reflectivity to SMAP soil moisture," *Geophys. Res. Lett.*, vol. 45, no, 9, pp. 4049–4057, May 2018.

[6] S. V. Nghiem *et al.*, "Wetland monitoring with global navigation satellite system reflectometry," *Earth Space Sci.*, vol. 4, no. 1, pp. 16–39, Jan. 2017.

[7] M. P. Clarizia, N. Pierdicca, F. Costantini, and N. Floury, "Analysis of CYGNSS data for soil moisture retrieval," *IEEE J. Sel. Top. Appl. Earth Obs. Remote Sens.*, vol. 12, no. 7, pp. 2227–2235, Jul. 2019.

[8] F. T. Ulaby, R. K. Moore, and A. K. Fung, *Microwave Remote Sensing: Active and Passive*, vol. 1. Reading, MA, USA: Addison-Wesley, 1981.

[9] M. M. Al-Khaldi, J. T. Johnson, A. J. O'Brien, A. Balenzano, and F. Mattia, "Time-series retrieval of soil moisture using CYGNSS," *IEEE Trans. Geosci. Remote Sens.*, vol. 57, no. 7, pp. 4322–4331, Jul. 2019, doi: 10.1109/TGRS.2018.2890646.

[10] A. M. Balakhder, M. M. Al-Khaldi, and J. T. Johnson, "On the coherency of ocean and land surface specular scattering for GNSS-R and signals of opportunity systems," *IEEE Trans. Geosci. Remote Sens.*, vol. 57, no. 12, pp. 10426–10436, Dec. 2019, doi: 10.1109/TGRS.2019.2935257.

[11] M. Unwin, P. Jales, J. Tye, C. Gommenginger, G. Foti, and J. Rosello, "Spaceborne GNSS-reflectometry on techdemosat-1: Early mission operations and exploitation," *IEEE J. Sel. Topics Appl. Earth Obs. Remote Sens.*, vol. 9, no. 10, pp. 4525–4539, Oct. 2016, doi: 10.1109/JSTARS.2016.26038461.

[12] C. S. Ruf *et al.*, "New ocean winds satellite mission to probe hurricanes and tropical convection," *Bull. Amer. Meteorol. Soc.*, vol. 97, no. 3, pp. 385–395, 2015.

[13] J. Wickert *et al.*, "GEROS-ISS: GNSS reflectometry, radio occultation, and scatterometry onboard the international space station," *IEEE J. Sel. Topics Appl. Earth Obs. Remote Sens.*, vol. 9, no. 10, pp. 4552–4581, Oct. 2016, doi: 10.1109/JSTARS.2016.2614428.

[14] M. Martin-Neira, M. Caparrini, J. Font-Rossello, S. Lannelongue, and C. Serra Vallmitjana, "The PARIS concept: An experimental demonstration of sea surface altimetry using GPS reflected signals," *IEEE Trans. Geosci. Remote Sens.*, vol. 39, no. 1, pp. 142–150, Jan. 2001.

[15] P. Ferrazzoli, L. Guerriero, N. Pierdicca, and R. Rahmoune, "Forest biomass monitoring with GNSS-R: Theoretical simulations'," *Adv. Space Res.*, vol. 47, pp. 1823–1832, 2011, doi: 10.1016/j.asr.2010.04.025.

[16] P. Liang, L. E. Pierce, and M. Moghaddam, "Radiative transfer model for microwave bistatic scattering from forests canopies," *IEEE Trans. Geosci. Remote Sens.*, vol. 43, no. 11, pp. 2470–2483, Nov. 2005.

[17] A. Egido *et al.*, "Global navigation satellite systems reflectometry as a remote sensing tool for agriculture," *Remote Sens.*, vol. 4, pp. 2356–2372, 2012, doi: 10.3390/rs4082356.

[18] A. Egido *et al.*, "Airborne GNSS-R soil moisture and above ground biomass observations," *IEEE J. Sel. Topics Appl. Earth Obs. Remote Sens.*, vol. 7, no. 5, pp. 1522–1532, May 2014.

[19] M. Zribi *et al.*, "Performance of GNSS-R GLORI data for biomass estimation over the landes forest," *Int. J. Appl. Earth Obs. Geoinf.*, vol. 74, pp. 150–158, 2019.

[20] M. C. Dobson, F. T. Ulaby, T. LeToan, A. Beaudoin, E. S. Kasischke, and N. Christensen, "Dependence of radar backscatter on coniferous forest biomass," *IEEE Trans. Geosci. Remote Sens.*, vol. 30, no. 2, pp. 412–415, Mar. 1992.

[21] H. Carreno-Luengo, A. Camps, J. Querol, and G. Forte, "First results of a GNSS-R experiment from a stratospheric balloon over boreal forests," *IEEE Trans Geosci. Remote Sens.*, vol. 54, no. 5, pp. 2652–2663, May 2016.

[22] A. Camps *et al.*, "Sensitivity of GNSS-R spaceborne observations to soil moisture and vegetation," *IEEE J. Sel. Topics Appl. Earth Obs. Remote Sens.*, vol. 9, no. 10, pp. 4730–4741, Oct. 2016.

[23] H. Carreno-Luengo, G. Luzi, and M. Crosetto, "Sensitivity of CyGNSS bistatic reflectivity and SMAP microwave radiometry brightness temperature to geophysical parameters over land surfaces," *IEEE J. Sel. Topics Appl. Earth Obs. Remote Sens.*, vol. 12, no. 1, pp. 107–122, Jan. 2019.

[24] H. Carreno-Luengo, G. Luzi, and M. Crosetto, "Biomass estimation over tropical rainforests using GNSS-R on-board the CyGNSS microsatellites constellation," in *Proc. Int. Geosci. Rem. Sens. Symp.*, 2019, pp. 8676–8679.

[25] A. Camps, M. Vall·llossera, H. Park, G. Portal, and L. Rossato, "Sensitivity of TDS-1 GNSS-R reflectivity to soil moisture: Global and regional differences and impact of different spatial scales," *Remote Sens.*, vol. 10, 2018, Art. no. 1856.

[26] P. E. O'Neill, S. Chan, E. G. Njoku, T. Jackson, and R. Bindlish, "SMAP L3 radiometer global daily 36 km EASE-grid soil moisture, Version 5," Boulder, CO, USA, NASA National Snow & Ice Data Center Distributed Active Center, 2018.

[27] V. Avitabile *et al.*, "An integrated pan-tropical biomass maps using multiple reference datasets," *Global Change Biol.*, vol. 22, pp. 1406–1420, 2016, doi: 10.1111/gcb.13139.

[28] M. Simard, N. Pinto, J. B. Fisher, and A. Baccini, "Mapping forest canopy height globally with spaceborne lidar," *J. Geophys. Res.*, vol. 116, 2011, Art. no. G04021, doi: 10.1029/2011JG001708.

[29] N. Pierdicca, L. Guerriero, R. Giusto, M. Brogioni, and A. Egido, "SAVERS: A simulator of GNSS reflections from bare and vegetated soils," *IEEE Trans. Geosci. Remote Sens.*, vol. 52, no. 10, pp. 6542–6554, Oct. 2014.

[30] A. Alonso-Arroyo *et al.*, "On the correlation between GNSS-R Reflectivity and L-band microwave radiometry," *IEEE J. Sel. Topics Appl. Earth Obs. Remote Sens.*, vol. 9, no. 12, pp. 5862–5879, Dec. 2016.

[31] S. J. Katzberg, O. Torres, M. S. Grant, and D. Masters, "Utilizing calibrated GPS reflected signals to estimate soil reflectivity and dielectric constant: Results from SMEX02," *Remote Sens. Environ.*, vol. 100, pp. 17–28, 2006.

[32] C. Chew, R. Shah, C. Zuffada, G. Hajj, D., Masters, and A. J. Mannucci, "Demonstrating soil moisture remote sensing with observations from the UK TechDemoSat-1 satellite mission," *Geophys. Res. Lett.*, vol. 43, pp. 3317–3324, 2016.

[33] H. Kim and V. Lakshmi, "Use of cyclone global navigation satellite system (CyGNSS) observations for estimation of soil moisture," *Geophys. Res. Lett.*, vol. 45, no. 16, pp. 8272–8282, 2018.

[34] O. Eroglu, O. M. Kurum, and J. Ball, "Response of GNSS-R on dynamic vegetated terrain conditions," *IEEE J. Sel. Topics Appl. Earth Obs. Remote Sens.*, vol. 12, no. 5, pp. 1599–1611, May 2019.

[35] N. Pierdicca *et al.*, "Spaceborne GNSS reflectometry data for land applications: An analysis of techdemosat data," in *Proc. Int. Geosci. Remote Sens. Symp.*, 2018, pp. 3343–3346.

[36] A. Camps, "Spatial resolution in GNSS-R under coherent scattering," *IEEE Geosci. Remote Sens. Lett.*, vol. 17, no. 1, pp. 32–36, Jan. 2020.

[37] D. Comite, F. Ticconi, L. Dente, L. Guerriero, and N. Pierdicca, "Bistatic coherent scattering from rough soils with application to GNSS reflectometry," *IEEE Trans. Geosci. Remote Sens.*, vol. 58, no. 1, pp. 612–625, Jan. 2020, doi: 10.1109/TGRS.2019.2938442.

[38] S. Gleason, "Level 1B DDM calibration algorithm theoretical basis document," CYGNSS Project Document 148-0137-X1, Rev., vol. 1, no. 19, Dec. 2014.

[39] A. G. Konings, M. Piles, N. Das, and D. Entekhabi, "L-band vegetation optical depth and effective scattering albedo estimation from SMAP," *Remote Sens. Environ.*, vol. 198, pp. 460–470, 2017, doi: doi.org/10.1016/j.rse.2017.06.037.

[40] T. Mo, B. J. Choudhury, T. J. Schmugge, J. R. Wang, and T. J. Jackson, "A model for microwave emission from vegetation covered fields," *J. Geophys. Res.*, vol. 87, pp. 11229–11237, 1982.

[41] A. Baccini, A. Laporte, N. S. J. Goetz, M. Sun, and H. Dong, "A first map of tropical Africa's above-ground biomass derived from satellite imagery," *Environ. Res. Lett.*, vol. 3, no. 4, 2008, Art. no. 045011.

[42] S. S. Saatchi *et al.*, "Benchmark map of forest carbon stocks in tropical regions across three continents," *Proc. Nat. Acad. Sci.*, vol. 108, no. 24, pp. 9899–9904, 2011.

[43] L. Breiman, "Random forests," *Mach. Learn.*, vol. 45, pp. 5–32, 2001.

[44] S. Bontemps *et al.*, "Consistent global land cover maps for climate modeling communities: Current achievements of the ESA's land cover CCI," in *Proc. ESA Living Planet Symp.*, Sep. 9–13, 2013.

[45] M. Tedesco and J. Jeyaratnam. "AMSR-E/AMSR2 unified L3 global daily 25 km EASE-Grid snow water equivalent," Version 1, Boulder, CO, USA, NASA National Snow and Ice Data Center Distributed Active Archive Center, 2019.

[46] C. Vittucci, P. Ferrazzoli, Y. Kerr, P. Richaume, G. Vaglio Laurin, and L. Guerriero, "Analysis of vegetation optical depth and soil moisture retrieved by SMOS over tropical forests," *IEEE Trans. Geosci. Remote Sens. Lett.*, vol. 16, no. 4, pp. 504–508, Apr. 2019, doi: 10.1109/LGRS.2018.2878359.

[47] C. Vittucci, G. Vaglio Laurin, G. Tramontana, P. Ferrazzoli, L. Guerriero, and D. Papale, "Vegetation optical depth at 1 band and above ground biomass in the tropical range: evaluating their relationships at continental and regional scales," *Int. J. Appl. Earth Obs. Geoinf.*, vol. 77, pp. 151–171, 2019.

[48] K. Hornik, "Multilayer feed forward network are universal approximators," *Neural Netw.*, vol. 2, no. 5, pp. 359–366, 1989.

[49] A. Linden and J. Kinderman, "Inversion of multi-layer nets," in *Proc. Int. Joint Conf. Neural Netw.*, vol. 2, 1989, pp. 425–43.

[50] N. Baghdadi, S. Gaultier, and C. King, "Retrieving surface roughness and soil moisture from synthetic aperture radar (SAR) data using neural networks," *Can. J. Remote Sens.*, vol. 28, no. 5, pp. 701–711, 2002, doi: 10.5589/m02-066.

[51] F. Del Frate, P. Ferrazzoli, and G. Schiavon, "Retrieving soil moisture and agricultural variables by microwave radiometry using neural networks," *Remote Sens. Environ.*, vol. 84, no. 2, pp. 174–183, 2003, doi: 10.1016/S0034-4257(02)00105-0.

[52] A. Elshorbagy and K. Parasuraman, "On the relevance of using artificial neural networks for estimating soil moisture content," *J. Hydrol.*, vol. 362, pp. 1–18, Nov. 30, 2008.

[53] X. Dai, Z. Huo, and H. Wang, "Simulation for response of crop yield to soil moisture and salinity with artificial neural network," *Field Crops Res.*, vol. 121, no. 3, pp. 441–449, 2011, doi: 10.1016/j.fcr.2011.01.016.

[54] E. Santi, "Neural networks applications for the remote sensing of hydrological parameters," in *Artificial Neural Networks—Models and Applications Book*. Berlin, Germany: TechOpen, 2016, ch. 12, pp. 309–334.

[55] E. Santi, S. Paloscia, S. Pettinato, and G. Fontanelli, "Application of artificial neural networks for the soil moisture retrieval from active and passive microwave spaceborne sensors," *Int. J. Appl. Earth Observ. Geoinf.*, vol. 48, pp. 61–73, 2016, doi: 10.1016/j.jag.2015.08.002.

Laura Dente received the Laurea degree in physics from the University of Bari, Bari, Italy, in 2000 and the Ph.D. degree from the University of Twente, Enschede, The Netherlands, in 2016.

In 2002, she was a Young Graduate Trainee with ESA-ESTEC, The Netherlands, and from 2003 to 2006, as a Research Fellow with CNR-ISSIA, Italy, working on soil moisture and biomass retrieval from SAR data. From 2007 to 2012, she was a Trainee Research Assistant with the University of Twente, ITC Faculty, focusing on passive and active microwave remote sensing for soil moisture monitoring. Since 2016, she has been a Research Fellow with the University of Rome Tor Vergata, Rome, Italy, where her main interests are GNSS reflectometry and its application over land.

Nicolas Floury (Member, IEEE) received the Diplôme d'Ingénieur degree from the Ecole Nationale Supérieure des Télécommunications, Paris, France, in 1993, and the Ph.D. degree from the Université Paris 7 Denis Diderot, Paris, France, in 1999.

Since 1999, he has been with the European Space Research and Technology Centre, European Space Agency, Noordwijk, The Netherlands, where he is the Head of the Wave Interaction and Propagation Section. His research interests include signal processing and electromagnetic modeling applied to microwave interaction with natural media.
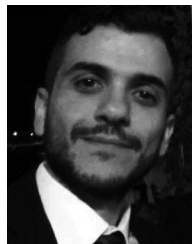
Maria Paola Clarizia (Senior Member, IEEE) received the master's degree in telecommunications engineering from the University of Sannio, Benevento, Italy, in 2007, and the Ph.D. degree in ocean remote sensing using GNSS-Reflectometry (GNSS-R) from the University of Southampton, Southampton, U.K., in 2012.

She has more than 10 years of experience in remote sensing, with a focus on GNSS-R, working in both academia and private industry. She has been a Research Engineer with Starlab, Barcelona, Spain, a Research Scientist with the National Oceanography Centre, Southampton, U.K., and a Postdoctoral Research Fellow with the University of Michigan, Ann Arbor, MI, USA, and with the University of Southampton, working on the National Aeronautics and Space Administration (NASA) Cyclone Global Navigation Satellite System (CYGNSS) Mission for ocean and land applications. She is currently a GNSS-R Technical Manager with Deimos Space, Harwell Oxford, U.K., and a member of the CYGNSS Science Team. Her current research interests include GNSS-reflectometry, altimetry and scatterometry, electromagnetic scattering models, retrieval algorithms, data analysis, and statistical processing.

Davide Comite (Member, IEEE) received the master's degree (*cum laude*) in telecommunications engineering and the Ph.D. degree in electromagnetics and mathematical models for engineering from the Sapienza University of Rome, Rome, Italy, in 2011 and 2015, respectively.

He was a Visiting Ph.D. Student with the Institute of Electronics and Telecommunications of Rennes, University of Rennes 1, Rennes, France, from March to June 2014, and a Postdoctoral Researcher with the Center of Advanced Communications, Villanova University, Villanova, PA, USA, from April to December 2015. He is currently a Postdoctoral Researcher with the Sapienza University of Rome. His research interests include the study of the scattering from natural surfaces as well as the GNSS reflectometry over the land, the microwave imaging and objects detection performed through GPR, the modeling of the radar signature in forward scatter radar systems, the study and design of leaky-wave antennas, and the generation of nondiffracting waves and pulses.

Dr. Comite has been a recipient of a number of research grants and awards. In 2019, the IEEE Antennas and Propagation Society recognized him as an Outstanding Reviewer for the IEEE TRANSACTIONS ON ANTENNAS AND PROPAGATION. He is currently a Reviewer for several international journals. He is an Associate Editor for the *IET Journal of Engineering*, *IET Microwaves, Antennas and Propagation* by the Institution of Engineering and Technology, and IEEE Access.

Nazzareno Pierdicca (Senior Member, IEEE) received the Laurea (Doctor's) (*cum laude*) degree in electronic engineering from the University "La Sapienza" of Rome, Rome, Italy, in 1981.

From 1978 to 1982, he was with the Italian Agency for Alternative Energy (ENEA). From 1982 to 1990, he was with Remote Sensing Division, Telespazio, Rome, Italy. In November 1990, he joined the Department of Information Engineering, Electronics and Telecommunications, Sapienza University of Rome, where he is currently a Full Professor and teaches remote sensing, antenna, and electromagnetic fields at the Faculty of Engineering. His research interests include electromagnetic scattering and emission models for sea and bare soil surfaces and their inversion, microwave radiometry of the atmosphere, SAR, bistatic radar, and GNSS-R land applications.

Prof. Pierdicca is a past Chairman of the GRSS Central Italy Chapter.

Simonetta Paloscia has been with the National Research Council (C.N.R.), since 1984. Since 2004, she has been scientific responsible of the Microwave Remote Sensing Group, IFAC-CNR (Institute of Applied Physics), and the research line "*Microwave Remote Sensing of natural surfaces*", in the EO Project of CNR. In 2010, she was nominated the Head of Research, National Research Council. She had a temporary teaching contract of "Microwave Remote Sensing Applications" for the Professional Master "Geomatics and Natural Resources Evaluation" at the "Istituto Agronomico per l'Oltremare" of the Ministry of Foreign Affairs in Florence from 1994 to 2010. She is the author and co-author of more than 100 works published on international journals and books, of more than 200 papers published on proceedings of international meetings. Her research currently focuses on the study of microwave emission and scattering of soil (bare and snow-covered) and vegetation.

She was PI and Co-I of many national and international projects (ASI, EC, ESA, and JAXA). Since 1996, she has been a Principal Investigator in JAXA Science Team of AQUA/AMSR-E and GCOM/AMSR-2 for algorithms development of soil moisture and vegetation biomass retrieval. She is member of the SMAP JPL/NASA Science Team. She was member of organizing and steering committees of international meetings (Specialist Meeting on Microwave Radiometry and IGARSS). She is member of the permanent Steering Committee of MicroRad Meeting and she was General Co-Chair of the MicroRad 1999 and 2008 and URSI-F 2010 meetings organized in Florence. She is an Associate Editor for the *International Journal of Remote Sensing*, IEEE JOURNAL OF SELECTED TOPICS IN APPLIED EARTH OBSERVATIONS AND REMOTE SENSING, and *European Journal of Remote Sensing*. She has been a URSI Fellow since 2020. She was the Vice-Chair and Chair of URSI Commission F from 2011 to 2017.

Leila Guerriero (Member, IEEE) received the Laurea degree in physics from Sapienza University of Rome, Italy, in 1986, and the Ph.D. degree in electromagnetism from Tor Vergata University of Rome, Rome, Italy, in 1991.

Since 1994, she has been a Permanent Researcher with Tor Vergata University, where she is currently an Associate Professor holding the courses on Earth Satellite Observation and on geoinformation. Her research interests include modeling microwave scattering and emissivity from agricultural and forested areas. She participated in several international projects, among them are the ESA projects Soil Moisture and Ocean Salinity Satellite, Development of SAR Inversion Algorithms for Land Applications, Use of Bistatic Microwave Measurements for Earth Observation, and SAOCOM-CS Bistatic Imaging, Radiometry and Interferometry Over Land. Lately, she has been involved in the modeling of Global Navigation Satellite System Reflectometry (GNSS-R) signals for ESA projects and in the European FP7 and H2020 Programmes.

Prof. Guerriero is a member of the Permanent Steering Scientific Committee of MicroRad. She is Secretary of the GRSS North-Central Italy Chapter.

Giacomo Fontanelli was born in Vinci, Florence, Italy, on July 8, 1976. He received the B.Sc. and M.Sc. degrees in forest and environmental science from the University of Florence, Florence, Italy, in 2007, a post-university degree in CAD-CAM technologies in 2010, and the Ph.D. degree in methods and technologies for environmental monitoring from the University of Basilicata, Potenza, Italy, in 2014.

Since 2009, he has been working with CNR- IFAC, Florence, Italy, working on GIS technologies for many European Research Projects. Since the end of 2013, he has been a Postdoctoral Researcher with CNR-IREA Institute, Milan, Italy, working on the SPACE4AGRI Project, in cooperation with the Lombardy Region. He joined Rothamsted in 2016, as an Agro-Environmental Scientist, involved in an Innovate U.K. program named "Advancing EO Application in Agriculture." In 2018, he came back to Italy and joined CNR-IFAC, working on the OPTIMED Project (Optimizing Water Management for Cultivated Lands through Remote Sensing Analyses and Climate Change Scenarios) leading the in situ campaigns and managing the GIS database. His current research focuses on providing useful information to farmers using RS data, in order to help them in agricultural practices and decision making.

Simone Pettinato (Member, IEEE) was born in Florence, Italy, in 1972. He received the M.S. degree in telecommunications engineering from the University of Florence, Florence, Italy, in 2002 and the Ph.D. degree in "methods and technologies for environmental monitoring" from the University of Basilicata, Potenza, Italy, in 2007.

Since 2003, he has been with the Microwave Remote Sensing Group, CNRIFAC, Florence, Italy, as a Scientist. He participated, as a Co-Investigator, in different national and international scientific projects funded by the European Community, European, and Italian Space agencies (ESA and ASI). Between 2009 and 2012, he was involved in three Antarctic expeditions in the framework of the DOMEX-2, DOMEX-3, and GPS-SIDS projects. He is the author or coauthor of more than 100 papers published on international peer-reviewed journals and conference proceedings. His research focuses on the investigation of the natural surfaces by means of active and passive microwave sensors in order to retrieve information of geophysical parameters related to the hydrological cycle (soil moisture, snow, and vegetation).

Emanuele Santi (Member, IEEE) received the M.S. degree in electronic engineering in 1997, from the University of Florence, Florence, Italy, and the Ph.D. degree in earth's remote sensing techniques from University of Basilicata, Potenza, Italy, in 2005.

Since 1998, he has been a Researcher with the Microwave Remote Sensing Group, Institute of Applied Physics of the National Research Council, Rome, Italy. He was and is currently involved in many national and international projects (ASI, EC, ESA, and JAXA), acting as a team leader, WP leader or co-I. He is the author or coauthor of 142 papers, published in ISI journals and books and conference proceedings. His research focuses of the development and validation of models and statistical inversion algorithms for estimating the geophysical parameters of soil, sea, snow, and vegetation from microwave emission and scattering.

Dr. Santi, in 2018, was the recipient of the "IEEE GRSS J-STARS Prize Paper Award" for the best paper published in the IEEE JOURNAL OF SELECTED TOPICS IN APPLIED EARTH OBSERVATIONS AND REMOTE SENSING in 2017. He is a member of the Institute of Electric and Electronic Engineers (IEEE) and the "Centro di Telerilevamento a Microonde (Microwave Remote Sensing Center)." He is also Conference Chair of the SPIE Europe Remote Sensing.